

Finite nuclei description from an effective relativistic parametrization based on nuclear matter DBHF calculations

M. Del Estal, M. Centelles, X. Viñas and S.K. Patra

*Departament d'Estructura i Constituents de la Matèria, Facultat de Física,
Universitat de Barcelona, Diagonal 647, E-08028 Barcelona, Spain*

Abstract

A relativistic mean field parameter set is constructed aiming to describe the energy density of nuclear matter derived in Dirac–Brueckner–Hartree–Fock theory and the properties of finite nuclei as well. We place the emphasis on the role of the new meson self-interactions and couplings that arise in the framework of the energy density expansion consistent with effective field theory recently suggested in the literature. We compare our calculations with other relativistic nuclear force parameters and study various nuclear phenomena. The results of the new parametrization agree well with the experimental data.

PACS: 21.60.-n, 21.10.Dr, 21.65.+f, 21.30.Fe

Keywords: Relativistic mean field approach, Dirac-Brueckner-Hartree-Fock, Nuclear structure, Non-linear self-interactions, Effective field theory

1 Introduction

One of the most challenging problems in nuclear physics is the description of finite nuclei starting from first principles. The bare nucleon–nucleon (NN) force has to be specified and then applied to finite nuclei calculations. This is a very complicated many-body problem which requires several simplifications to be affordable. The understanding of the bare NN interaction has been a current subject of study almost since the beginning of nuclear physics [1]. The last generation of modern potentials, like the Bonn [1] or Nijmegen [2] potential, based on meson-exchange models give a very accurate description of the deuteron properties and NN scattering up to laboratory energies around 300 MeV.

These NN forces are also applied to study nuclear matter where rather complicated many-body techniques must be used. The non-relativistic Brueckner–Goldstone calculations based on realistic NN potentials are not able to give, at the same time, the right saturation density and binding energy of nuclear matter (Coester line) [3]. To obtain the correct values, an additional repulsive part has to be added. This additional density-dependent term, although described some times as a relativistic effect, can at least partially be understood in terms of three and many-body forces [4].

The agreement between empirical and calculated data in nuclear matter is considerably improved by working in the relativistic framework. The extension of the two-nucleon problem to nuclear matter in the relativistic domain is done using the so-called Dirac–Brueckner–Hartree–Fock (DBHF) theory [5,6,7,8,9] that goes beyond mean field incorporating two-body correlations. The DBHF calculations show two essential features. On the one hand, the rather small effect of the two-body correlations on the large mean field scalar and vector self-energies. On the other hand, the momentum dependence of the scalar and time-like self-energies is small and they can be considered to be almost constant for occupied states in the Fermi sea. The DBHF calculations introduce an extra density dependence, not included in the non-relativistic Brueckner–Goldstone approach, that allows to fit simultaneously the NN phase shifts and the nuclear matter equilibrium point [1,7].

All these properties of the DBHF calculations in nuclear matter suggest the possibility of fitting the scalar and time-like DBHF self-energies as well as the binding energy in nuclear

matter by a much simpler relativistic mean field approach. One can expect that the fitted parameters will retain to some extent the effect of the two-body correlations. This strategy was carried out in the past using the non-linear $\sigma-\omega$ model with scalar [10] and vector self-interactions [11] and was applied to finite nuclei calculations. Another possible way to perform finite nuclei calculations starting from DBHF results in nuclear matter consists of using a linear $\sigma-\omega$ Lagrangian where the scalar and vector coupling constants are, actually, functions of the nuclear density ρ [12].

Following Refs. [11] and [13], Sugahara and Toki [14] utilised the quartic vector self-coupling to improve the relativistic force parameters. They constructed two parameter sets, TM1 and TM2, for finite nuclei. The TM2 parameter set was designed for atomic number $Z \leq 20$ and the TM1 set for larger charge number. They also calculated the equation of state as well as the structure of neutron star and supernovae using the TM1 parameter set [14,15]. TM1 gave good results for several finite nuclei properties and showed a better agreement with the DBHF calculations for nuclear matter made with the Bonn-A potential [16] than the conventional non-linear $\sigma - \omega$ parametrizations (such as NL1 [17] or NL-SH [18]) because of the vector self-interaction.

The recent description of quantum hadrodynamics (QHD) [19] as an effective field theory which includes new scalar-vector interactions plus tensor couplings of the ω and ρ mesons to the nucleon [4,20,21], motivates us to repeat the analysis on the basis of DBHF calculations with the new effective Lagrangian. Our aim is to study the importance of the additional couplings and to evaluate whether they contribute to improve already established parametrizations such as TM1 [14]. Particularly, TM1 offers a very good starting point due to its predictive power for nuclear matter and finite nuclei properties. We will base our analysis in investigating whether the TM1 parameter set completed with the new couplings can produce better results for both nuclear matter and finite nuclei. In the next section we will detail our strategy. It is worthwhile to mention that the NL-RA parameter set of Ref. [10] and the parametrizations by Gmuca [11] do not properly reproduce the known properties of finite nuclei.

It should be pointed out that the new extended Lagrangians also contain $\sigma - \rho$ meson

interactions, as well as terms with gradients of the scalar and vector fields. Of course, the coupling constants associated to these interactions cannot be obtained from a DBHF calculation in symmetric nuclear matter. We will adjust these coupling constants, related with the finite size and asymmetry of nuclei, to reproduce several properties of some selected doubly magic nuclei.

Although the mean field approach in its simplest (Hartree) version that we use here does not contain exchange terms or the contributions of antiparticles to the sources of the mesonic fields, it is expected that these effects as well as the contributions from two-body correlations will be included in a phenomenological way in the meson masses and coupling constants of the effective Lagrangian [22].

The paper is organized as follows. The next section is devoted to a summary of the mean field equations and to fit some of the parameters of the effective Lagrangian to the nuclear matter DBHF data [16]. We compare our results with the predictions of other parametrizations available in literature. In the third section the remaining parameters of the effective Lagrangian are obtained by imposing that our mean field approach reproduces the experimental data for some selected nuclei. We compare the results obtained with the new parameter set for magic nuclei. The BCS type pairing correlation is added in Section 4 to study the properties of even-even finite nuclei beyond the closed shell. The new parameter set is used to study some nuclear structure phenomena, like the isotopic/isotonic energy differences, the isotopic change in the charge radius and nuclei near the drip lines. Finally, the summary and concluding remarks are given in Section 5.

2 The mean field approach: nuclear matter description

QHD has been widely used in the relativistic treatment of nuclear systems during recent years. The simple σ - ω model of Walecka [19] and its non-linear extensions with cubic and quartic self-interactions of the scalar meson field [23] have been usually preferred to this end. The model contains Dirac nucleons together with neutral scalar and vector mesons, as well as isovector-vector ρ mesons. It is able to reproduce nuclear matter and finite nuclei data [14,22,17] with a quality comparable to the one found in non-relativistic nuclear structure calculations with effective Skyrme [24] or Gogny [25] forces. The success of this model lies on the fact that at the mean field (Hartree) level it already contains the spin-orbit force, the finite range and the density dependence which are essential ingredients of the nuclear force.

Recently, this model has been generalized by including other non-linear interactions among the meson fields and tensor couplings on the basis of effective field theories [4,20,21]. The effective theory contains all the non-renormalizable couplings consistent with the underlying symmetries of QCD. Therefore, one has to deal with an effective Lagrangian with an infinite number of terms and, thus, it is imperative to develop a suitable truncation scheme. In the nuclear many-body problem, the scalar (Φ) and vector (W) meson fields are small as compared with the nucleon mass, at least for densities around saturation. On the other hand, the meson fields vary slowly in finite nuclei. This means that the ratios Φ/M , W/M , $|\nabla\Phi|/M^2$ and $|\nabla W|/M^2$ are the useful expansion parameters in the nuclear effective theory [4,20,21,26]. The concept of naturalness [21], i.e., that all the coupling constants written in an appropriate dimensionless form should be of order unity, is used to avoid ambiguities in the development.

Following Ref. [20], the meson field equations can be derived from an energy density functional containing Dirac baryons and classical scalar and vector mesons. Although this energy functional can be obtained from the effective Lagrangian in the Hartree approximation [4,21], it can also be considered as an expansion in terms of ratios of the meson fields

and their gradients to the nucleon mass of a general energy density functional that contains the contributions of correlations within the spirit of density functional theory.

According to Refs. [4,20,21] this energy density functional for finite nuclei can be written as

$$\begin{aligned}
\mathcal{E}(r) = & \sum_{\alpha} \varphi_{\alpha}^{\dagger}(r) \left\{ -i\boldsymbol{\alpha} \cdot \boldsymbol{\nabla} + \beta[M - \Phi(r)] + W(r) + \frac{1}{2}\tau_3 R(r) + \frac{1 + \tau_3}{2} A(r) \right. \\
& - \frac{i\beta\boldsymbol{\alpha}}{2M} \cdot \left(f_v \boldsymbol{\nabla} W(r) + \frac{1}{2} f_{\rho} \tau_3 \boldsymbol{\nabla} R(r) \right) \left. \right\} \varphi_{\alpha}(r) \\
& + \left(\frac{1}{2} + \frac{\kappa_3}{3!} \frac{\Phi(r)}{M} + \frac{\kappa_4}{4!} \frac{\Phi^2(r)}{M^2} \right) \frac{m_s^2}{g_s^2} \Phi^2(r) - \frac{\zeta_0}{4!} \frac{1}{g_v^2} W^4(r) \\
& + \frac{1}{2g_s^2} \left(1 + \alpha_1 \frac{\Phi(r)}{M} \right) (\boldsymbol{\nabla} \Phi(r))^2 - \frac{1}{2g_v^2} \left(1 + \alpha_2 \frac{\Phi(r)}{M} \right) (\boldsymbol{\nabla} W(r))^2 \\
& - \frac{1}{2} \left(1 + \eta_1 \frac{\Phi(r)}{M} + \frac{\eta_2}{2} \frac{\Phi^2(r)}{M^2} \right) \frac{m_v^2}{g_v^2} W^2(r) \\
& - \frac{1}{2g_{\rho}^2} (\boldsymbol{\nabla} R(r))^2 - \frac{1}{2} \left(1 + \eta_{\rho} \frac{\Phi(r)}{M} \right) \frac{m_{\rho}^2}{g_{\rho}^2} R^2(r), \tag{2.1}
\end{aligned}$$

where the index α runs over all occupied states of the positive energy spectrum, $\Phi \equiv g_s \phi_0$, $W \equiv g_v V_0$, $R \equiv g_{\rho} b_0$ and $A \equiv e A_0$. Except for the terms with α_1 and α_2 , the functional (2.1) is of fourth order in the expansion. The fifth-order terms α_1 and α_2 are retained because their contribution has been estimated to be numerically of the same magnitude as the quartic scalar term in the nuclear surface energy [4,21,26].

The mean field equations for Φ , W , R and A are given by

$$\begin{aligned}
-\Delta \Phi(r) + m_s^2 \Phi(r) = & g_s^2 \rho_s(r) - \frac{m_s^2}{M} \Phi^2(r) \left(\frac{\kappa_3}{2} + \frac{\kappa_4}{3!} \frac{\Phi(r)}{M} \right) \\
& + \frac{g_s^2}{2M} \left(\eta_1 + \eta_2 \frac{\Phi(r)}{M} \right) \frac{m_v^2}{g_v^2} W^2(r) + \frac{\eta_{\rho}}{2M} \frac{g_s^2}{g_{\rho}^2} m_{\rho}^2 R^2(r) \\
& + \frac{\alpha_1}{2M} [(\boldsymbol{\nabla} \Phi(r))^2 + 2\Phi(r)\Delta \Phi(r)] + \frac{\alpha_2}{2M} \frac{g_s^2}{g_v^2} (\boldsymbol{\nabla} W(r))^2, \tag{2.2} \\
-\Delta W(r) + m_v^2 W(r) = & g_v^2 \left(\rho(r) + \frac{f_v}{2} \rho_T(r) \right) - \left(\eta_1 + \frac{\eta_2}{2} \frac{\Phi(r)}{M} \right) \frac{\Phi(r)}{M} m_v^2 W(r)
\end{aligned}$$

$$-\frac{1}{3!}\zeta_0 W^3(r) + \frac{\alpha_2}{M}[\nabla\Phi(r) \cdot \nabla W(r) + \Phi(r)\Delta W(r)], \quad (2.3)$$

$$-\Delta R(r) + m_\rho^2 R(r) = \frac{1}{2}g_\rho^2 \left(\rho_3(r) + \frac{1}{2}f_\rho \rho_{\text{T},3}(r) \right) - \eta_\rho \frac{\Phi(r)}{M} m_\rho^2 R(r), \quad (2.4)$$

$$-\Delta A(r) = e^2 \rho_{\text{p}}(r), \quad (2.5)$$

where the baryon, scalar, isovector, proton and tensor densities are

$$\rho(r) = \sum_{\alpha} \varphi_{\alpha}^{\dagger}(r) \varphi_{\alpha}(r), \quad (2.6)$$

$$\rho_{\text{s}}(r) = \sum_{\alpha} \varphi_{\alpha}^{\dagger}(r) \beta \varphi_{\alpha}(r), \quad (2.7)$$

$$\rho_3(r) = \sum_{\alpha} \varphi_{\alpha}^{\dagger}(r) \tau_3 \varphi_{\alpha}(r), \quad (2.8)$$

$$\rho_{\text{p}}(r) = \sum_{\alpha} \varphi_{\alpha}^{\dagger}(r) \left(\frac{1 + \tau_3}{2} \right) \varphi_{\alpha}(r), \quad (2.9)$$

$$\rho_{\text{T}}(r) = \sum_{\alpha} \frac{i}{M} \nabla \cdot \left[\varphi_{\alpha}^{\dagger}(r) \beta \boldsymbol{\alpha} \varphi_{\alpha}(r) \right], \quad (2.10)$$

$$\rho_{\text{T},3}(r) = \sum_{\alpha} \frac{i}{M} \nabla \cdot \left[\varphi_{\alpha}^{\dagger}(r) \beta \boldsymbol{\alpha} \tau_3 \varphi_{\alpha}(r) \right]. \quad (2.11)$$

In the context of density functional theory it is possible to parametrize the exchange and correlation effects through local potentials (Kohn–Sham potentials), as long as those contributions be small enough that can be considered as minor perturbations to the potentials [27]. As it is known, this is the case with the local meson fields. Clearly, the Hartree values are the ones that control the dynamics in the relativistic DBHF calculations. Therefore, we can also interpret the meson fields as Kohn–Sham potentials. Equations (2.2)–(2.5) thus correspond to the Kohn–Sham equations in the relativistic case [28]. In this sense they include effects beyond the Hartree approach through the non-linear couplings [20,21].

For infinite nuclear matter all of the gradient contributions in Eqs. (2.1)–(2.5) vanish and only the κ_3 , κ_4 , η_1 , η_2 and ζ_0 non-linear couplings remain. Due to the fact that the properties of nuclear matter at the mean field level do not depend on the the coupling constants g_{s} and g_{v} and the meson masses independently but only on the ratios $g_{\text{s}}^2/m_{\text{s}}^2$ and $g_{\text{v}}^2/m_{\text{v}}^2$, we have seven parameters to fit to nuclear matter properties. By imposing the values of the

saturation density, total energy, incompressibility modulus and effective mass, we still have three free parameters.

In particular, the vector meson quartic self-interaction (ζ_0) was introduced by Bodmer [13]. It allows one to avoid the negative sign in the quartic self-interaction (κ_4) which appears in many non-linear σ - ω parametrizations that correctly reproduce finite nuclei, though they can lead to a pathological behaviour of the scalar potential in some special situations. On the other hand, the equation of state is softened at moderate high densities when the vector non-linearity is taken into account. This effect has been used by Gmuca [11] for fitting DBHF results in nuclear matter. An excellent starting point for the study of the effects of the new terms in the extended effective Lagrangians, as mentioned in the Introduction, is the TM1 parametrization [14]. First, because TM1 reproduces the DBHF calculations with the Bonn-A potential with a very good agreement for low and moderate nuclear densities. And second, because it provides good results when applied to the calculation of finite nuclei properties, even far away from the β -stability line.

Thus, it seems a natural choice to fix the saturation properties of TM1 and to introduce on top of them the new mixed scalar-vector non-linear couplings η_1 and η_2 . This way we can make sure, broadly speaking, that we have the same behaviour of the equation of state around the saturation point as with TM1. It is important to note that the introduction of the couplings η_1 and η_2 cannot be done with complete freedom because we have fixed the saturation properties. This is translated into a modification of the other coupling constants which, eventually, can move to non-natural values. A more extended discussion of this effect can be found in Ref. [26]. To keep all the coupling constants within natural values, η_1 and η_2 should lie in a narrow region around unity. We find that $\eta_1 = 2$ and $\eta_2 = 1$ is a good choice, because it provides a good reproduction of the DBHF results keeping the coupling constants in the natural region. We must point out that we are not trying to find a strictly best new fit. As it can be seen from semi-infinite nuclear matter calculations [26], the fine tuning for finite nuclei calculations can be done with all the other couplings which average to zero in nuclear matter. The values of the coupling constants entering the mean field nuclear matter calculation along with the saturation properties are collected in Table 1. From this table

we can see that κ_4 is positive and that all the coupling constants are natural. The value of κ_4 is somehow high but still acceptable. We have denoted this set of parameters as TM1*.

Figure 1 displays the scalar U_s and vector U_v potentials as a function of the nuclear matter density calculated with TM1*, TM1 (that only contains quartic vector self-interactions) and with the generalized sets G1 and G2 of Ref. [21], in comparison with the DBHF result. Figure 2 shows the DBHF equation of state compared with its mean field approach calculated in the same cases as in Figure 1. From these figures it is clear that the cubic and quartic self-interactions play a crucial role in the fit of the DBHF results at high density. By construction, TM1* gives at the saturation density the same nuclear matter properties as TM1. However, due to the presence of the mixed meson-meson interactions η_1 and η_2 , the DBHF results are better reproduced by TM1* than by TM1, for moderate and high densities. The nuclear matter results of the G1 and G2 sets (that were obtained by fitting twenty-nine finite nuclei observables) [4,21] also show a good agreement with the DBHF results. From Figures 1 and 2 one can see that the results obtained with G1 are similar to the TM1 ones while the predictions of G2 are closer to the DBHF results.

3 Finite nuclei description

In finite nuclei the contributions from the couplings α_1 and α_2 between the scalar field and the gradients of the vector and scalar fields, as well as the tensor couplings f_v and f_ρ of the ω and ρ mesons to the nucleon, do not cancel. Therefore, we have in principle four new parameters for adjusting finite nuclei properties, plus the scalar mass m_s . In the same spirit in which we are building the TM1* parameter set, we will fix m_s to the same value as in TM1. It is the best way to do not mask the influence of the terms that we want to study. Similarly, for finite nuclei the constants g_v , g_s and g_ρ are independent from the masses of the ω , σ and ρ mesons. To be consistent with our strategy we choose the masses m_v , m_s and m_ρ to be equal to the ones of Ref. [14] for TM1: 783 MeV, 511.198 MeV and 770 MeV respectively (the nucleon mass is $M = 938$ MeV).

Starting from Eq. (2.1) the variation with respect to φ_α^\dagger gives the Dirac equation

$$\left\{ -i\boldsymbol{\alpha}\cdot\nabla + \beta[M - \Phi(r)] + W(r) + \frac{1}{2}\tau_3 R(r) + \frac{1+\tau_3}{2}A(r) - \frac{i\beta\boldsymbol{\alpha}}{2M}\cdot\left[f_v\nabla W(r) + \frac{1}{2}f_\rho\tau_3\nabla R(r)\right] \right\} \varphi_\alpha(r) = \varepsilon_\alpha \varphi_\alpha(r). \quad (3.1)$$

If spherical symmetry is assumed, the spinor corresponding to a level α is characterized by the single-particle angular momentum quantum numbers j_α and m_α , the parity Π_α and the isospin $t_\alpha = \pm\frac{1}{2}$ [19,22]:

$$\varphi_\alpha(\mathbf{r}, s, t) = \begin{pmatrix} f_\alpha(r)\mathcal{Y}_{j_\alpha l_\alpha m_\alpha}(\theta, \varphi, s) \\ ig_\alpha(r)\mathcal{Y}_{j_\alpha \bar{l}_\alpha m_\alpha}(\theta, \varphi, s) \end{pmatrix} \chi_{t_\alpha}, \quad (3.2)$$

where $\mathcal{Y}_{j_\alpha l_\alpha m_\alpha}(\theta, \varphi, s)$ are the generalized spherical harmonics, χ_{t_α} is an isospinor and

$$\begin{aligned} l_\alpha &= j_\alpha + \frac{1}{2} & \bar{l}_\alpha &= j_\alpha - \frac{1}{2} & \text{for } \Pi &= (-1)^{j_\alpha + \frac{1}{2}}, \\ l_\alpha &= j_\alpha - \frac{1}{2} & \bar{l}_\alpha &= j_\alpha + \frac{1}{2} & \text{for } \Pi &= (-1)^{j_\alpha - \frac{1}{2}}. \end{aligned} \quad (3.3)$$

This way, the Dirac equation (3.1) splits in two coupled first-order differential equations:

$$\begin{aligned} [M - \Phi(r) + W(r)] f_\alpha(r) + \left\{ \partial_r - \frac{\kappa_\alpha - 1}{r} + \frac{1}{2M} \left(f_v \frac{\partial W(r)}{\partial r} + f_\rho \frac{\partial R(r)}{\partial r} \right) \right\} g_\alpha(r) \\ = \varepsilon_\alpha f_\alpha(r), \end{aligned} \quad (3.4)$$

$$\begin{aligned}
& - [M - \Phi(r) - W(r)] g_\alpha(r) - \left\{ \partial_r + \frac{\kappa_\alpha - 1}{r} + \frac{1}{2M} \left(f_v \frac{\partial W(r)}{\partial r} + f_\rho \frac{\partial R(r)}{\partial r} \right) \right\} f_\alpha(r) \\
& = \varepsilon_\alpha g_\alpha(r), \quad (3.5)
\end{aligned}$$

where $\kappa_\alpha = \pm(j_\alpha + \frac{1}{2})$ for $j_\alpha = l_\alpha \mp \frac{1}{2}$.

Instead of using a harmonic oscillator basis for solving Eqs. (3.4) and (3.5) [22], we have transformed them into a Schrödinger-like equation by eliminating the small component $g_\alpha(r)$. The equation is solved by using a standard code for non-relativistic Skyrme–Hartree–Fock calculations [24]. To take into account the center-of-mass correction, we use a harmonic oscillator estimate which gives a simplified correction [22]:

$$E_{\text{CM}} = \frac{3}{4} \hbar \omega, \quad \hbar \omega = 41 A^{-1/3} \text{ MeV}. \quad (3.6)$$

First, we obtain the coupling constants α_1 , α_2 and f_v by imposing that the total energy, the charge radii and the 1p and 1d splittings of the ^{16}O and ^{40}Ca nuclei be as close as possible to the experimental values. In a second step, and using these α_1 and α_2 values, we fix η_ρ and f_ρ in such a way that the energies of ^{48}Ca and ^{208}Pb be the experimental ones. Nevertheless, the tensor coupling f_ρ happens to be useless in this fitting. Its contribution, as previously reported [26,29], is negligible in the natural region of values of f_ρ and thus we have set $f_\rho = 0$ for TM1*. This is not the case for the coupling η_ρ , whose influence is noticeable [26]. Although this scheme should allow to obtain α_1 , α_2 , f_v , η_ρ and g_ρ , the additional constraint of naturalness imposes some limitations on the values of these coupling constants. The values which allow one to obtain a fit of the energies within $\sim 0.8\%$ in error and the splittings of ^{16}O , ^{40}Ca and ^{208}Pb with a similar quality to the one obtained using the G1 and G2 parametrizations [4,21] are reported in Table 1.

As a first test of the TM1* parametrization we have calculated in semi-infinite nuclear matter the surface energy coefficient E_s and the surface thickness t of the density profile (standard 90%-10% fall-off distance of the nuclear density). The results are shown in Table 2. The surface energy obtained with the TM1* parameter set lies within the region of empirical values, whereas the surface thickness t is slightly small [26,30].

The energies and charge radii $r_{\text{ch}} = \sqrt{r_p^2 + 0.64}$ (in fm) [22] of the magic nuclei ^{16}O , ^{40}Ca , ^{48}Ca and ^{208}Pb used in the fit of the coupling constants are displayed in Table 2, together

with the experimental values and those of TM1. We also show the results obtained with the NL-SH parameter set [18] that is chosen as a representative of the usual non-linear $\sigma-\omega$ parametrizations. Note that the κ_4 term of NL-SH bears a negative sign. We furthermore compare our results with the G1 and G2 parameter sets of Ref. [21]. In order to check the ability of the TM1* parametrization for describing nuclei far from the stability line, we have calculated the energy and charge radius of some drip-line nuclei, namely ^{56}Ni , ^{78}Ni , ^{100}Sn and ^{132}Sn . From Table 2 one can notice that all the forces produce similar results for finite nuclei. For example, the energy per particle is slightly overestimated by the TM1 set, while all the other parameter sets present similar results between each other. Similarly, the charge radius is quite close to the experimental data in all the parameter sets considered here. For light nuclei with $Z \leq 20$, we compared the binding energy given by the TM1* parametrization with the one of TM2 (as it is designed for $Z \leq 20$) and with the NL-SH result. TM1* produces similar values to the NL-SH parameter set, while the prediction of the TM2 parametrization is slightly better than with TM1*.

The calculated results on the total energies, single-particle energies and charge radii for ^{16}O and ^{40}Ca are tabulated in Table 3. For comparison, results of the relativistic density dependent Dirac-Hartree (RDDH) approach of Brockmann and Machleidt [12] are also shown. It is interesting to find that the results with the TM1* parameter set are very close to the experimental data. The improvements as compared to RDDH are remarkable. We have adjusted the total energy E almost perfectly. For example, the energies for ^{16}O and ^{40}Ca are 128.8 and 342.8 MeV, respectively, with the TM1* parameter set, whereas they are 120 and 320 MeV in the RDDH calculations, (the experimental values are 127.7 and 340 MeV). Similarly, the charge radius with TM1* is closer to the data than in the RDDH calculations.

The single-particle energies of neutrons and protons are compared with the experimental data in Figure 3 for the ^{208}Pb nucleus with the TM1, NL-SH and TM1* parameter sets. From this figure one can see that all these parametrizations qualitatively describe the experimental values. Although the nuclear matter properties are equal in TM1 and TM1*, the spectra is slightly different mainly due to the tensor coupling f_v in TM1* which is known to have a noticeable influence in the spin-orbit potential [4,20,26,31]. We also have calculated density

distributions with TM1 and TM1* for ^{40}Ca and ^{208}Pb and have found very similar results with both parameter sets.

4 Application to some nuclear structure phenomena: even-even nuclei beyond closed shells

Using Eqs. (3.4) and (3.5) we can only calculate closed shell nuclei. In order to describe even-even nuclei with open shells, we introduce the pairing correlation in the BCS approximation with a constant gap Δ , as in earlier calculations [14,22]. With this approach the densities (2.6)–(2.11) are replaced by sums weighted over the occupation probability

$$n_\alpha = \frac{1}{2} \left[1 + \frac{\varepsilon_\alpha - \lambda}{\sqrt{(\varepsilon_\alpha - \lambda)^2 + \Delta^2}} \right], \quad (4.1)$$

where λ is the chemical potential for neutrons or protons determined by imposing the condition

$$\sum_\alpha n_\alpha = N \text{ or } Z. \quad (4.2)$$

This schematic pairing contributes to the energy a quantity

$$E_{\text{pair}} = -\Delta \sum_\alpha \sqrt{n_\alpha(1 - n_\alpha)}. \quad (4.3)$$

In the constant gap approach the pairing energy diverges if the sum in (4.3) is extended over an infinite configuration space [22]. To avoid this, we restrict the number of active shells to the occupied shells contained in a major harmonic oscillator shell above and below of the last closed shell.

The constant gap Δ is adjusted to reproduce as well as possible the isotopic energy difference [33]

$$\Delta E = [E - E(^{116}\text{Sn})]_{\text{RMFBCS}} - [E - E(^{116}\text{Sn})]_{\text{Exp.}}, \quad (4.4)$$

assuming that ^{116}Sn has no pairing contribution. From this we find that the gap can be fitted to the phenomenological formula of Bohr and Mottelson [32] $\Delta = 11.2/\sqrt{A}$ (MeV), in agreement with the literature [14,17,22].

In the following subsections, we shall compare our results obtained with the TM1* parameter set with the result of different relativistic parametrizations and also with the experimental observations: we shall study isotopic and isotonic energy differences, isotopic

shifts in charge radii and two-neutron and two-proton separation energies near and away from the β -stability line.

4.1 Isotopic and isotonic energy differences

The isotopic energy differences ΔE for several Sn and Pb isotopes calculated with TM1*, TM1 and NL-SH are shown in Figures 4a and 4b. All the three parameter sets give qualitatively similar results for the Sn isotopic series. A careful analysis makes it clear that the results of the NL-SH parameter set deviate from experiment more remarkably than the predictions of TM1* and TM1 for the heavier isotopes. The TM1 parameter set gives better results for lower neutron number, see Figure 4a. Similar results for Pb isotopes are shown in Figure 4b and for $N = 82$ isotones in Figure 4c. The TM1*, TM1 and NL-SH parameter sets predict different conclusions for the isotopic energy differences for Pb isotopes. For example, TM1 predicts better ΔE values over the other two parameter sets. For lighter isotopes, the NL-SH set gives comparable results with TM1, while for heavier isotopes the results of NL-SH are not good (in comparison to TM1 and TM1*). On the other hand, the results of the TM1* parametrization are not encouraging for the whole $N = 82$ isotonic chain. The ΔE value is better for the NL-SH parameter set. However, the results obtained from the TM1* and TM1 parameter sets are almost similar and become worse at around the $Z = 55-60$ region.

4.2 Isotopic change in charge radius

Now we come to the result of the isotopic change in the charge radius. In the past years the isotopic shifts in charge radii have been studied for the isotopic chain of Pb nuclei [33,34,35] using various techniques. The standard non-relativistic forces (zero range or finite range forces) are not able to reproduce the experimentally observed kink in the isotopic shifts about ^{208}Pb . It has been shown [34] that the calculated shifts are very sensitive to the choice of the pairing interaction. The relativistic mean field calculations [35] are able to reproduce the data by changing some input parameters. As nuclear radii are sensitive to ground-state correlations [36], it may be a solution to use the effective character of the

interaction to slightly modify some of its parameters to improve the calculations. Here, we have calculated the Pb isotopic shifts with the TM1* parameter set. In Figure 5 the result is compared with the prediction of the TM1 and NL-SH parameter sets, and also with the experimental data. All the parameter sets yields qualitatively similar results and reproduce the experimentally observed kink reasonably well.

4.3 Two-neutron and two-proton separation energies

During the last decade there have been speculations about the neutron [37] and proton [38,39,40] halos in neutron-rich and proton-rich light nuclei. Actually, the nuclei considered for the candidature of a halo system are Li, Be and B nuclei, which have considerably smaller charge numbers than the nuclei we are considering here. For the larger neutron/proton numbers the formation of neutron/proton skins is rather more important. The quantity that plays a crucial role in the formation of a neutron/proton skin near the neutron-/proton-drip line is the two-neutron/proton separation energy. From the calculated energies we evaluated the two-neutron S_{2n} and two-proton S_{2p} energies using the relations [32]

$$S(N, Z)_{2n} = E(N, Z) - E(N - 2, Z) \quad (4.5)$$

and

$$S(N, Z)_{2p} = E(N, Z) - E(N, Z - 2), \quad (4.6)$$

respectively.

The S_{2n} values for the illustrative cases of $Z = 20$ and 82 as well as the S_{2p} value for $N = 82$ with the TM1*, NL-SH and TM1 sets are presented in Figures 6a, 6b and 6c, respectively. The experimental data are also given for comparisons. It is clear that the S_{2n} and S_{2p} values obtained from the TM1* parameter set agree well with the experimental observation and also with the predictions of TM1 and NL-SH (except for a slight discrepancy for some specific cases). On the whole, the TM1* parameter set reproduces quite well the experimental observations for the S_{2n} and S_{2p} energies. Here, all the parameter sets predict nearly similar results, agreeing quite well with the experimental data. The S_{2n}

value decreases with an increase of the neutron number and it vanishes at the neutron-drip line. Similarly, the S_{2p} value decreases with increasing proton number as it reaches the proton-drip line.

5 Summary and conclusions

In summary, we have explored whether the TM1 parameter set [14] can be improved (i.e., for nuclear matter without spoiling the predictive capability for finite nuclei) by adding new couplings that stem from the modern effective field theory approach to relativistic nuclear phenomenology. We have called this new parameter set TM1*. In fitting the DBHF results, TM1* shows a significant improvement over the TM1 parameter set, which only contains the quartic vector self-interaction, due to the addition of the η_1 and η_2 couplings. The latter couplings are very important to bring the vector and scalar potentials closer towards the DBHF calculations for high densities.

After getting the parameters for nuclear matter, then we have searched for a better parametrization by calculating finite nuclei systems. To this end we have introduced the f_v , α_1 , α_2 , η_ρ and f_ρ parameters on top of the TM1* set that describes nuclear matter (i.e., the TM1 set plus η_1 and η_2). The new parameters have a minor influence on the properties of finite nuclei. However, they allow the full TM1* parametrization to improve the agreement of the energies and charge radii with respect to the experimental values for double closed shell nuclei as compared with the starting TM1 parameter set. It is also important to mention that from a formal point of view the set TM1* is more satisfactory than the set TM1, because it includes the relevant couplings in the energy density expansion consistent with effective field theory developed in Refs. [4,21]. It is to be kept in mind that the TM1 parameter set was devised for nuclei with $Z > 20$, whereas our TM1* is a single parametrization for the whole atomic chart.

To extend the study for even-even nuclei apart from magic systems, we have included the BCS-type pairing correlation in a constant gap approach. After adjusting the gap parameter for TM1*, we have calculated two-neutron and two-proton separation energies, isotopic energy differences and isotopic changes in charge radii. These properties are explained

reasonably well by the new TM1* parameter set, with a quality similar to the one found with the most successful parametrizations.

From our analysis it is clear that the relativistic mean field approach worked out with the recently proposed extensions that contain new non-linear meson self-interactions and tensor couplings on the basis of effective field theory, allows one to fit at the same time DBHF data up to relatively high densities and finite nuclei properties. It is important to note that in the low density domain (that corresponds to the finite nuclei region) the main properties are almost fixed by the nuclear matter properties around the saturation density, and that the new parameters have only a small contribution. However, in the high density region the vector-vector and scalar-vector meson interactions play an important role in describing the DBHF results.

6 Acknowledgements

The authors would like to acknowledge support from the DGICYT (Spain) under grant PB95-1249 and from DGR (Catalonia) under grant 1998SGR-00011. M.D.E. acknowledges financial support from the CIRIT (Catalonia). S.K.P. thanks the Spanish Education Ministry grant SB97-OL174874 for financial support and the Departament d'Estructura i Constituents de la Matèria of the University of Barcelona for kind hospitality.

References

- [1] R. Machleidt, *Adv. Nucl. Phys.* 19 (1989) 189.
- [2] V.G. Stoks, R.A.M. Klomp, C.P.F. Terheggen and J.J. de Swart, *Phys. Rev. C* 49 (1994) 2950.
- [3] F. Coester, S. Cohen, B.D. Day and C.M. Vincent, *Phys. Rev. C* 1 (1970) 769.
- [4] B.D. Serot and J.D. Walecka, *Int. J. of Mod. Phys. E* 6 (1997) 515.
- [5] C.J. Horowitz and B.D. Serot, *Phys. Lett. B* 137 (1984) 283; *Nucl. Phys. A* 464 (1987) 613; *Nucl. Phys. A* 473 (1987) 760(E).
- [6] M.R. Anastasio, L.S. Celenza, W.S. Pong and C.M. Shakin, *Phys. Rep.* 100 (1983) 327.
- [7] R. Brockmann and R. Machleidt, *Phys. Lett. B* 149 (1984) 283; *Phys. Rev. C* 42 (1985) 1990.
- [8] B. ter Haar and R. Malfliet, *Phys. Rep.* 149 (1987) 207.
- [9] A. Amerim and J.A. Tjon, *Phys. Rev. Lett.* 68 (1992) 772.
- [10] M. Rashdan, *Phys. Lett. B* 395 (1997) 141.
- [11] S. Gmuca, *Z. Phys. A* 342 (1992) 387; *Nucl. Phys. A* 547 (1992) 447.
- [12] R. Brockmann and R. Machleidt, "Open problems in Nuclear Matter", (M. Baldo Ed. World Scientific, Singapore, 1997).
- [13] A.R. Bodmer, *Nucl. Phys. A* 526 (1991) 703; A.R. Bodmer and C.E. Price, *Nucl. Phys. A* 505 (1989) 123.
- [14] Y. Sugahara and H. Toki, *Nucl. Phys. A* 579 (1994) 557.
- [15] K. Sumiyoshi, H. Kuwabara and H. Toki, *Nucl. Phys. A* 581 (1995) 725.
- [16] R. Brockmann and R. Machleidt, *Phys. Rev. C* 42 (1990) 1965.
- [17] P.-G. Reinhardt, M. Rufa, J. Maruhn, W. Greiner and J. Friedrich, *Z. Phys. A* 323 (1986) 13.
- [18] M.M. Sharma, M.A. Nagarajan and P. Ring, *Phys. Lett. B* 312 (1993) 377.
- [19] B.D. Serot and J.D. Walecka, *Adv. Nucl. Phys.* 16 (1986) 1.
- [20] R.J. Furnstahl, B.D. Serot and H.B. Tang, *Nucl. Phys. A* 598 (1996) 539.

- [21] R.J. Furnstahl, B.D. Serot and H.B. Tang, Nucl. Phys. A 615 (1997) 441.
- [22] Y.K. Gambhir, P. Ring and A. Thimet, Ann. Phys. (N.Y.) 198 (1990) 132.
- [23] J. Boguta and A.R. Bodmer, Nucl. Phys. A 292 (1977) 413.
- [24] D. Vautherin and D.M. Brink, Phys. Rev. C 5 (1972) 626.
- [25] J. Dechargé and D. Gogny, Phys. Rev. C 21 (1980) 1568.
- [26] M. Del Estal, M. Centelles and X. Viñas, Nucl. Phys. A 650 (1999) 443
- [27] W. Kohn and L.J. Sham, Phys. Rev. A 140 (1965) 1133.
- [28] C. Speicher, R.M. Dreizler and E. Engel, Ann. Phys. (N.Y.) 213 (1992) 413
- [29] M. Rufa, P.-G. Reinhard, J.A. Maruhn, W. Greiner and M.R. Strayer, Phys. Rev. C 38 (1988) 390.
- [30] M. Centelles and X. Viñas, Nucl. Phys. A 563 (1993) 173; M. Centelles, M. Del Estal and X. Viñas, Nucl. Phys. A 635 (1998) 193.
- [31] R.J. Furnstahl, J.J. Rusnak and B.D. Serot, Nucl. Phys. A 632 (1998) 607.
- [32] A. Bohr and B.R. Mottelson, “Nuclear Structure”, Vol. I (W.A. Benjamin, New York 1969), Ch. 2.
- [33] E. Chabanat, P. Bonche, P. Haensel, J. Meyer and R. Schaeffer, Nucl. Phys. A 635 (1998) 231.
- [34] N. Tajima, P. Bonche, H. Flocard, P. -H. Heenen and M.S. Weiss, Nucl. Phys. A 551 (1993) 434.
- [35] M.M. Sharma, G.A. Lalazissis and P. Ring, Phys. Lett. B 317 (1993) 9.
- [36] P. -G. Reinhard and M. Girod, Nucl. Phys. A 389 (1982) 179.
- [37] I. Tanihata, J. Phys. G22 (1996) 157.
- [38] T. Minamisono, T. Ohtsubo, I. Minami, S. Fukuda, A. Kitagawa, M. Fukuda, K. Matsuta, Y. Nojiri, S. Takeda, H. Sagawa and H. Kitagawa, Phys. Rev. Lett. 69 (1992) 2058.
- [39] H. Kitagawa and H. Sagawa, Phys. Lett. B299 (1993) 1.
- [40] S.K. Patra, Cheng-Li Wu and C.R. Praharaaj, Mod. Phys. Lett. A13 (1998) 2743.

Figure captions

Figure 1. Scalar U_s and vector U_v potentials against the nuclear matter density as obtained in a DBHF calculation with the Bonn-A potential [16] and with the relativistic mean field parametrizations TM1*, TM1 [14], G1 and G2 [21].

Figure 2. Equation of state for the same cases as in Figure 1.

Figure 3. The single-particle energies for ^{208}Pb obtained by various relativistic mean-field parametrizations are compared with the experimental data for neutrons (a) and protons (b).

Figure 4. The isotopic energy difference obtained with the TM1* parameter set is compared with the TM1 and NL-SH calculations for Sn isotopes (a) and Pb isotopes (b). Plot (c) shows the isotonic energy difference for $N = 82$.

Figure 5. The isotopic shifts in charge radii for the $Z = 82$ chain.

Figure 6. The calculated separation energies are compared with the experimental data: (a) two-neutron separation energy S_{2n} for $Z = 20$, (b) two-neutron separation energy for $Z = 82$, and (c) two-proton separation energy S_{2p} for $N = 82$.

Table 1: Various parameter sets for the relativistic energy density functional and the corresponding saturation properties. The coupling constants are dimensionless.

	TM1*	TM1	NL-SH	G1	G2
m_s/M	0.545	0.545	0.560	0.540	0.554
$g_s/4\pi$	-0.950	-0.798	-0.831	-0.785	-0.835
$g_v/4\pi$	1.319	1.003	1.03	0.9650	1.015
κ_3	3.676	1.021	0.886	2.201	3.247
κ_4	15.544	0.124	-2.774	-10.090	0.631
ζ_0	0.872	2.689	0.0	3.525	2.642
η_1	2.0	0.0	0.0	0.071	0.650
η_2	1.0	0.0	0.0	-0.961	0.110
α_1	0.35	0.0	0.0	1.855	1.723
α_2	-1.50	0.0	0.0	1.788	-1.580
$f_v/4$	0.05	0.0	0.0	0.108	0.173
η_ρ	-0.35	0.0	0.0	-0.722	0.390
a_v (MeV)	-16.30	-16.30	-16.35	-16.14	-16.07
ρ_∞ (fm ⁻³)	0.145	0.145	0.146	0.153	0.153
K (MeV)	281.1	281.1	355.3	215.0	215.0
M_∞^*/M	0.634	0.634	0.598	0.634	0.664
J (MeV)	36.90	36.90	36.12	38.5	36.4

Table 2: The surface energy coefficient E_s , surface thickness t , energy per nucleon E/A , charge radius r_{ch} and spin-orbit splitting in energy ΔE_{SO} using the TM1*, TM1, NL-SH, G1 and G2 parameter sets are compared with the experimental data. The energies are given in MeV, while t and r_{ch} are given in fm. The experimental values of E/A for ⁷⁸Ni and ¹⁰⁰Sn are, in fact, extrapolated data [33].

Table 2

		TM1*	TM1	NL-SH	G1	G2	Exp.
	E_s	18.49	18.51	18.96	18.06	17.80	16.5–21.0
	t	1.85	1.91	1.83	1.98	2.08	2.2–2.5
^{16}O	E/A	−8.05	−8.15	−8.04	−8.08	−8.08	−7.98
	r_{ch}	2.69	2.71	2.71	2.75	2.77	2.73
	ΔE_{SO} (n)	6.3	5.6	6.8	6.0	6.0	6.2
	(p)	6.2	5.6	6.7	6.0	6.0	6.3
^{40}Ca	E/A	−8.57	−8.61	−8.51	−8.52	−8.54	−8.55
	r_{ch}	3.43	3.46	3.46	3.48	3.49	3.48
	ΔE_{SO} (n)	6.2	5.7	6.9	6.6	6.5	6.3
	(p)	6.2	5.7	6.8	6.6	6.5	7.2
^{48}Ca	E/A	−8.66	−8.65	−8.66	−8.65	−8.68	−8.67
	r_{ch}	3.46	3.48	3.47	3.49	3.50	3.47
	ΔE_{SO} (n)	5.1	5.0	6.2	5.8	5.6	3.6
	(p)	5.4	5.2	6.4	6.3	6.1	4.3
^{56}Ni	E/A	−8.59	−8.56	−8.64	−8.57	−8.58	−8.64
	r_{ch}	3.74	3.75	3.72	3.74	3.76	3.75
^{78}Ni	E/A	−8.21	−8.19	−8.26	−8.26	−8.29	−8.23
	r_{ch}	3.97	3.98	3.94	3.96	3.97	–
^{100}Sn	E/A	−8.29	−8.27	−8.31	−8.24	−8.24	−8.26
	r_{ch}	4.49	4.50	4.47	4.48	4.49	–
^{132}Sn	E/A	−8.35	−8.33	−8.39	−8.35	−8.36	−8.35
	r_{ch}	4.72	4.74	4.71	4.72	4.72	–
^{208}Pb	E/A	−7.87	−7.87	−7.89	−7.87	−7.86	−7.87
	r_{ch}	5.53	5.55	5.51	5.52	5.52	5.50
	ΔE_{SO} (n)	0.8	0.6	0.8	0.8	0.9	0.9
	(p)	1.6	1.4	1.7	1.8	1.8	1.3

Table 3: The energy per nucleon E/A , charge radius r_{ch} and single particle energies ε for the TM1* parameter set and the relativistic density dependent Hartree (RDDH) approach of Ref. [12] are compared with experiment for ^{16}O and ^{40}Ca . The single-particle energies ε for protons and neutrons are not separated in the RDDH values. The experimental single-particle energies are taken from Ref. [11]. The energies are in MeV and the radius is in fm.

		TM1*	RDDH	Exp.
^{16}O	E/A	-8.05	-7.5	-7.98
	r_{ch}	2.69	2.66	2.73
	$\varepsilon(1s_{1/2})$	-41.7 (n), -37.5 (p)	-43.5	-42.2 (n), -39.25(p)
	$\varepsilon(1p_{3/2})$	-22.3 (n), -18.4 (p)	-21.8	-22.86 (n), -18.6 (p)
	$\varepsilon(1p_{1/2})$	-16.0 (n), -12.2 (p)	-16.5	-16.22 (n), -12.98 (p)
^{40}Ca	E/A	-8.57	-8.0	-8.55
	r_{ch}	3.43	3.36	3.48
	$\varepsilon(1s_{1/2})$	-52.2 (n), -44.1 (p)	-53.3	-61.5 (n), -53.6(p)
	$\varepsilon(1p_{3/2})$	-38.1 (n), -30.2 (p)	-36.0	-61.5 (n), -34.7 (p)
	$\varepsilon(1p_{1/2})$	-34.7 (n), -26.8 (p)	-32.0	-42.1 (n), -29.8 (p)
	$\varepsilon(1d_{5/2})$	-23.3 (n), -15.8 (p)	-19.3	-23.6 (n), -15.7 (p)
	$\varepsilon(1d_{3/2})$	-16.1 (n), -9.6 (p)	-13.6	-15.6 (n), -8.5 (p)
	$\varepsilon(2s_{1/2})$	-17.1 (n), -8.7 (p)	-14.3	-18.2 (n), -11.0 (p)

Figure 1

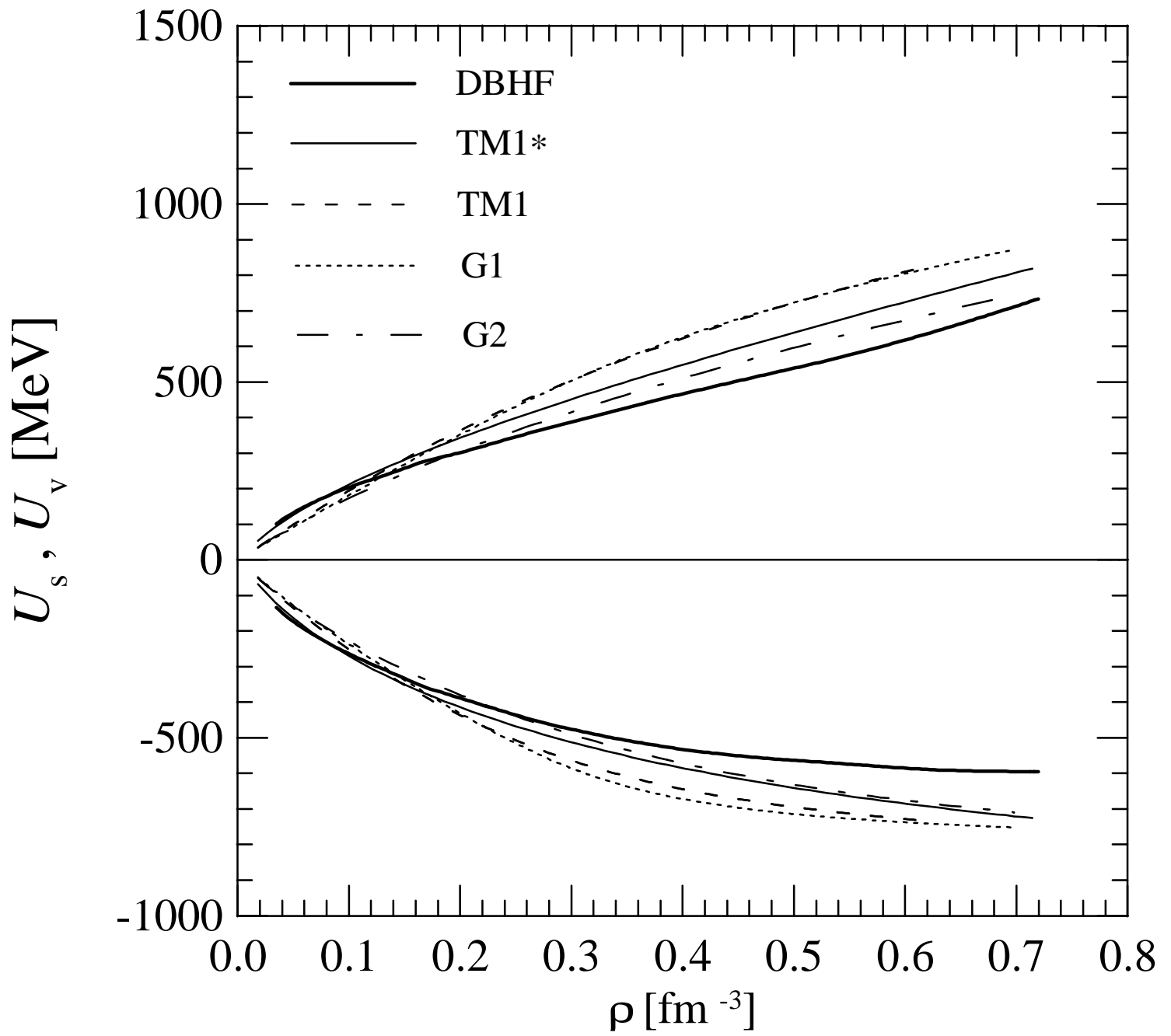


Figure 2

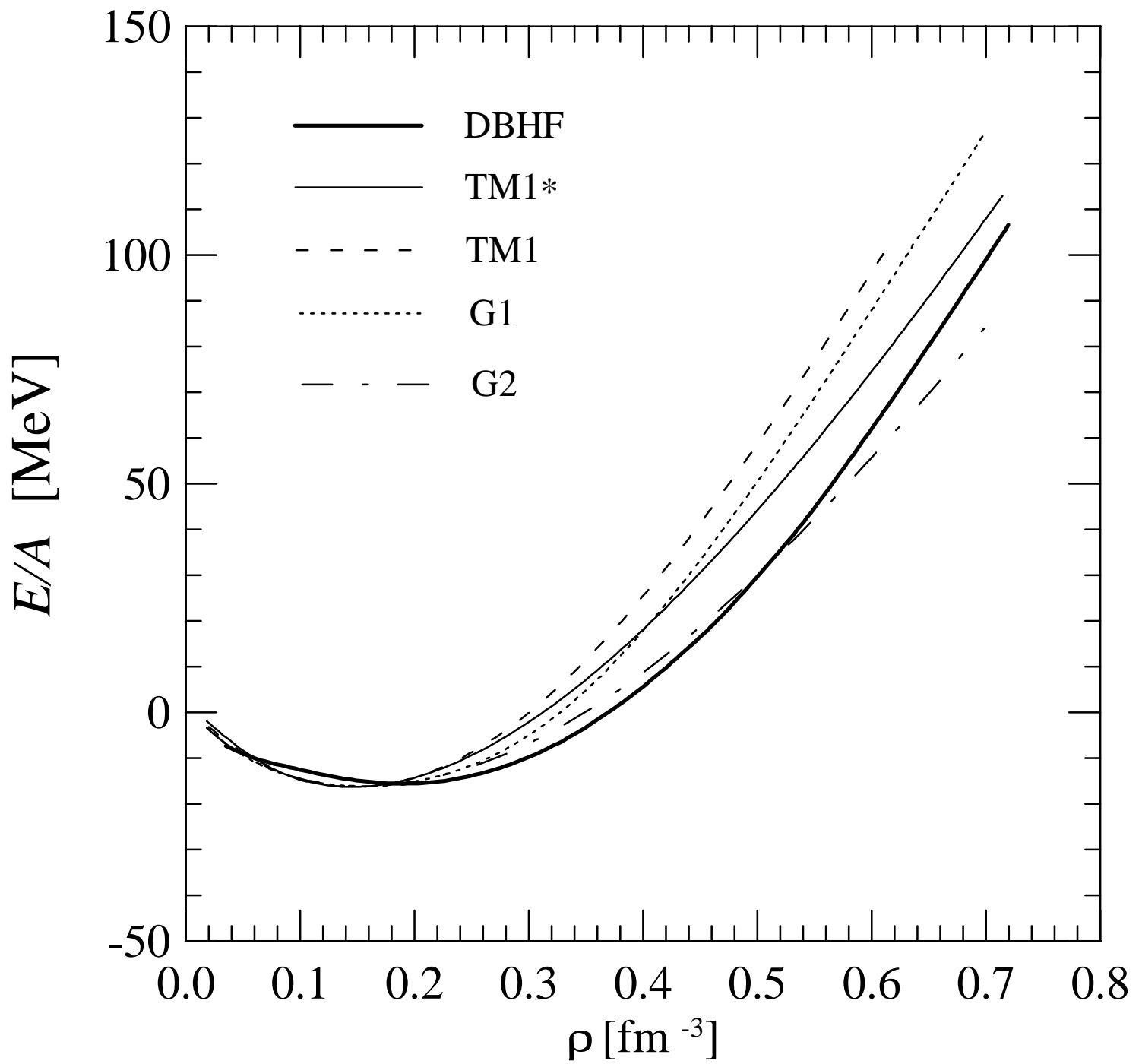


Figure 3a

^{208}Pb

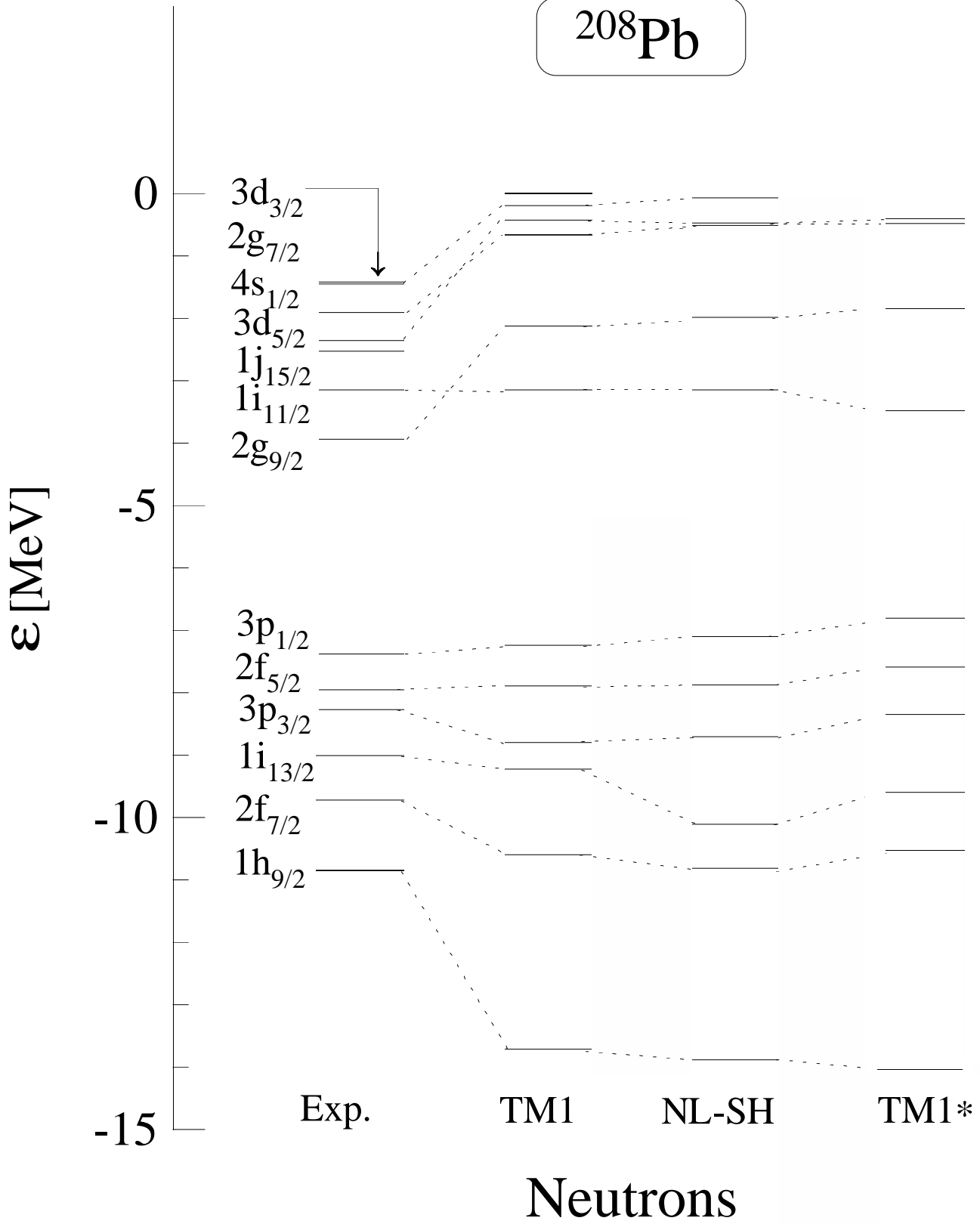


Figure 3b

^{208}Pb

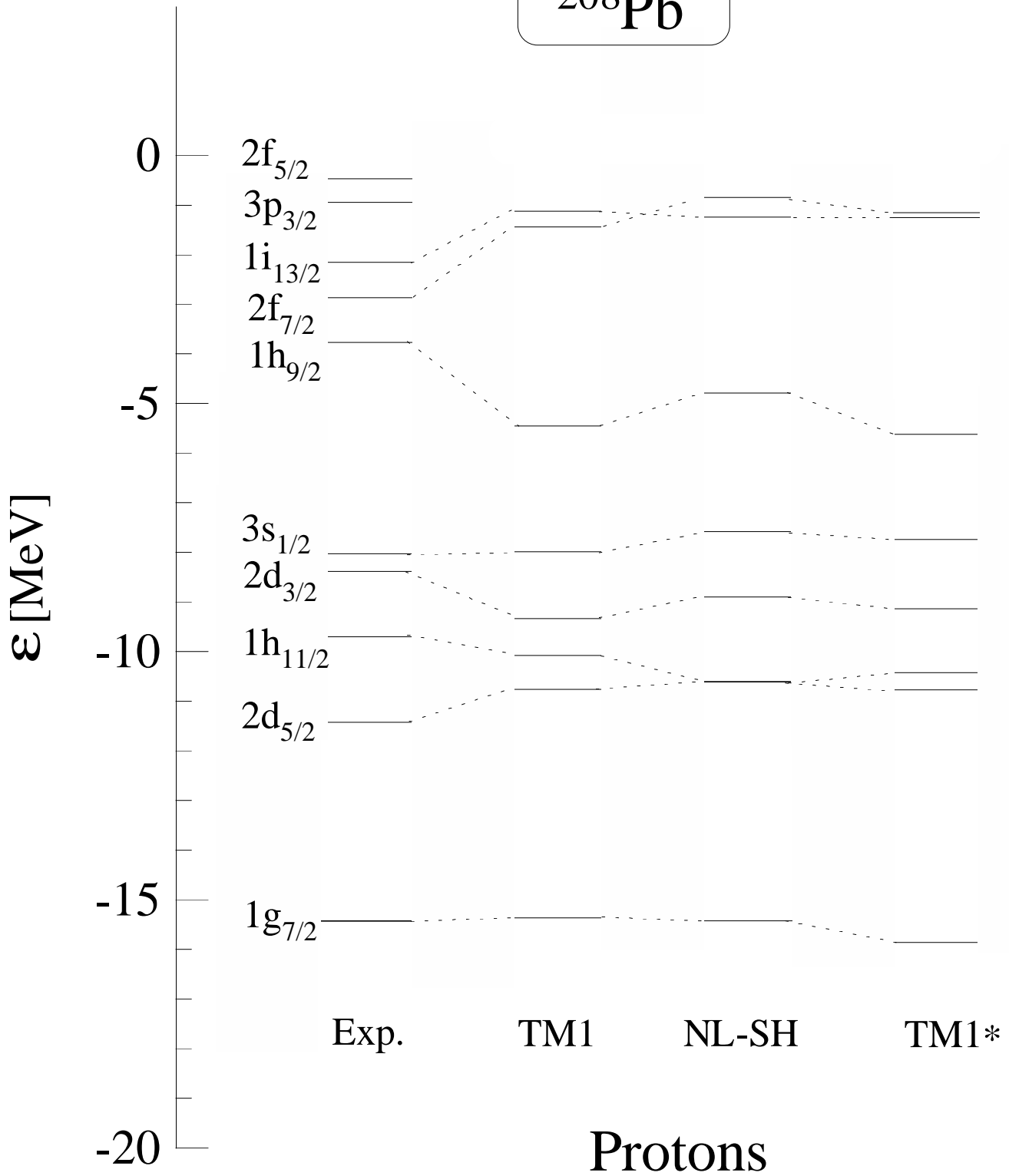


Figure 4a

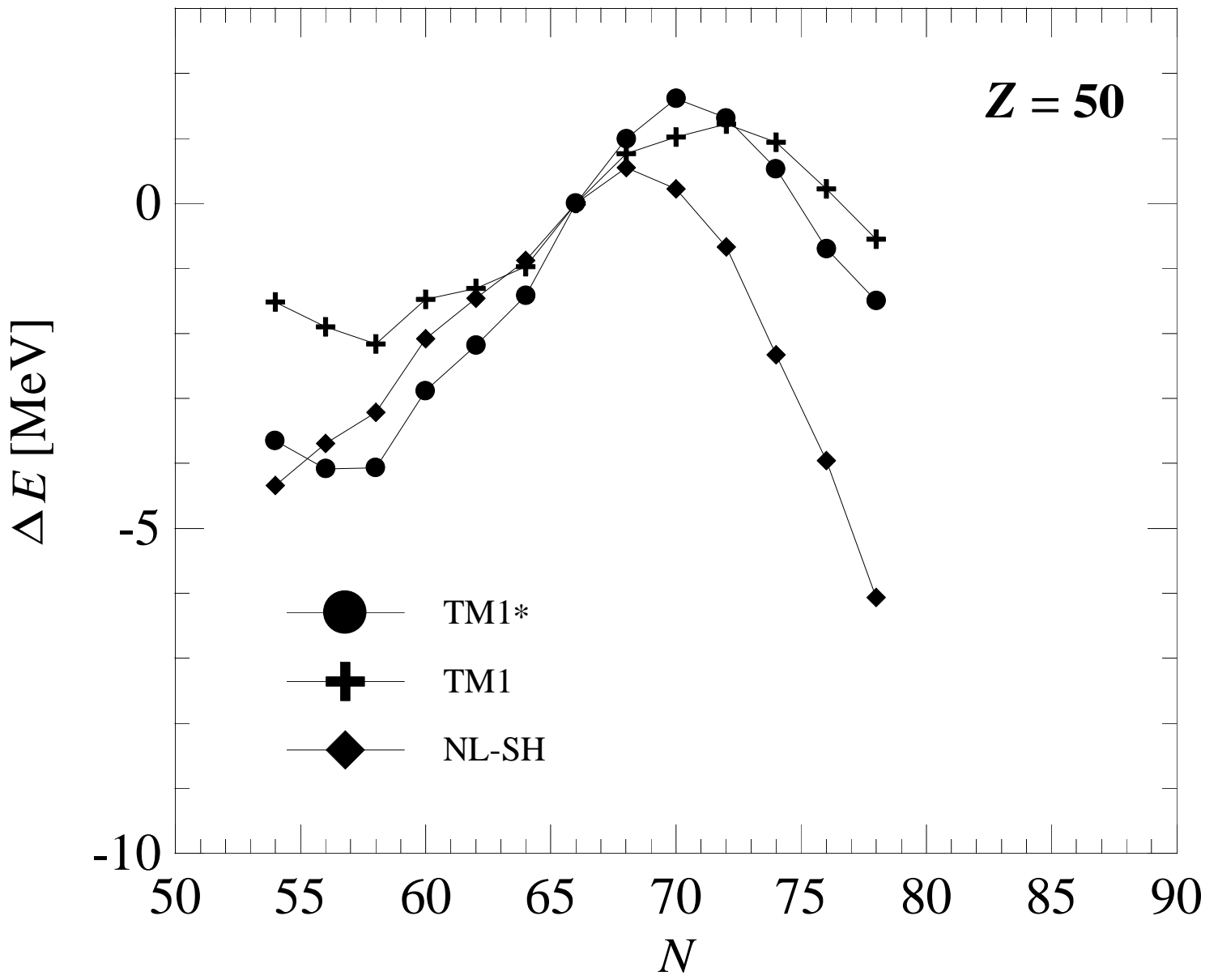


Figure 4b

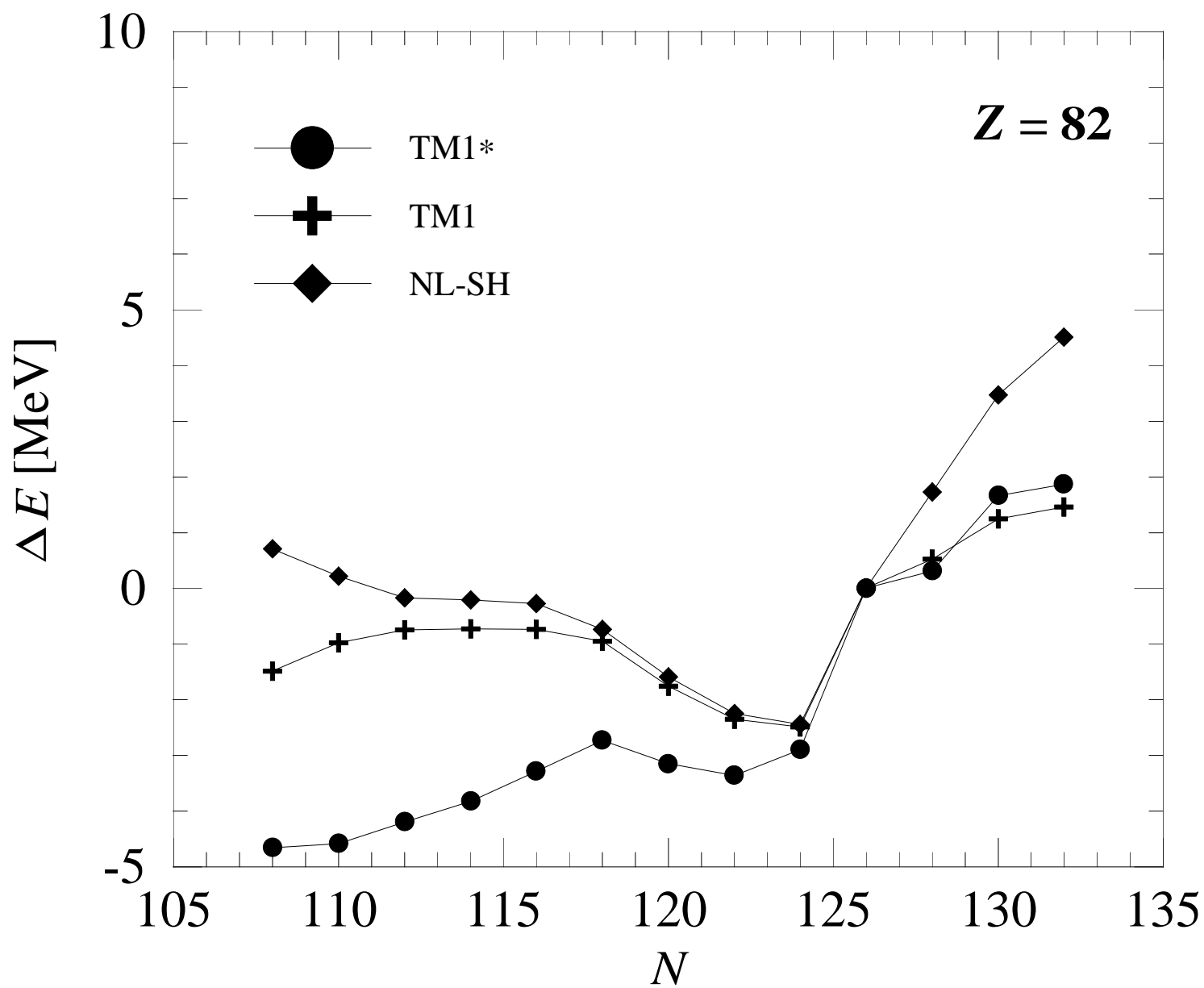


Figure 4c

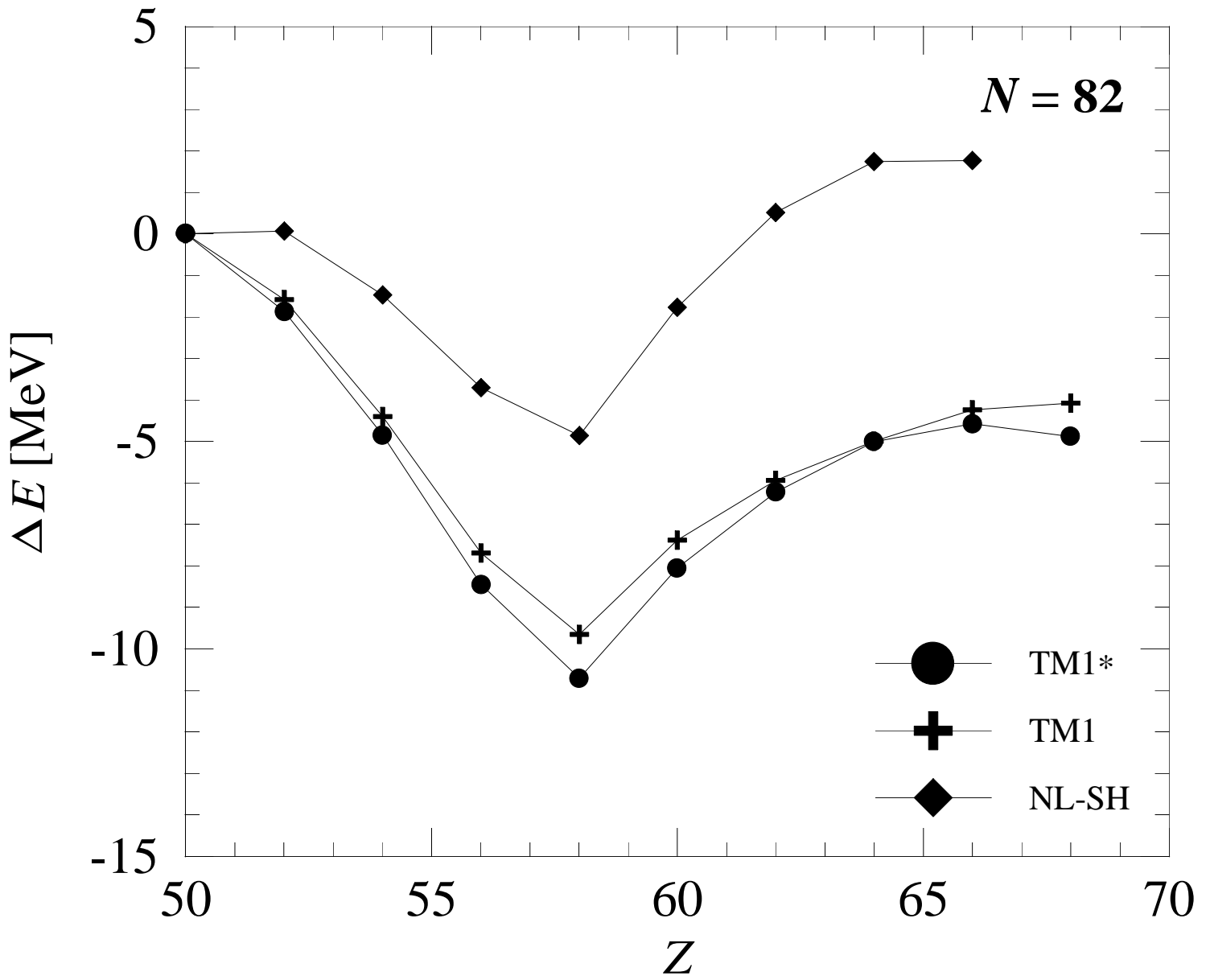


Figure 5

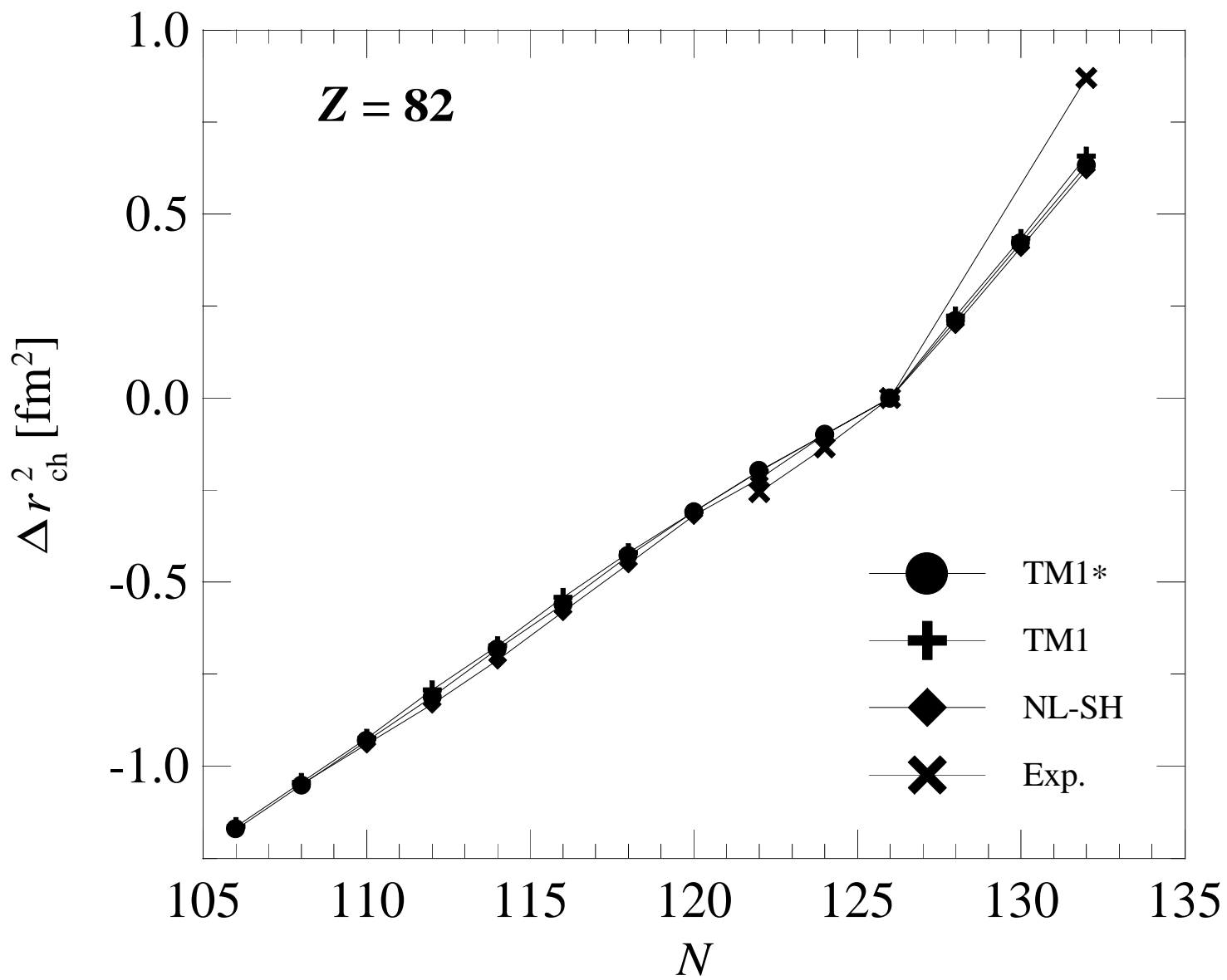


Figure 6a

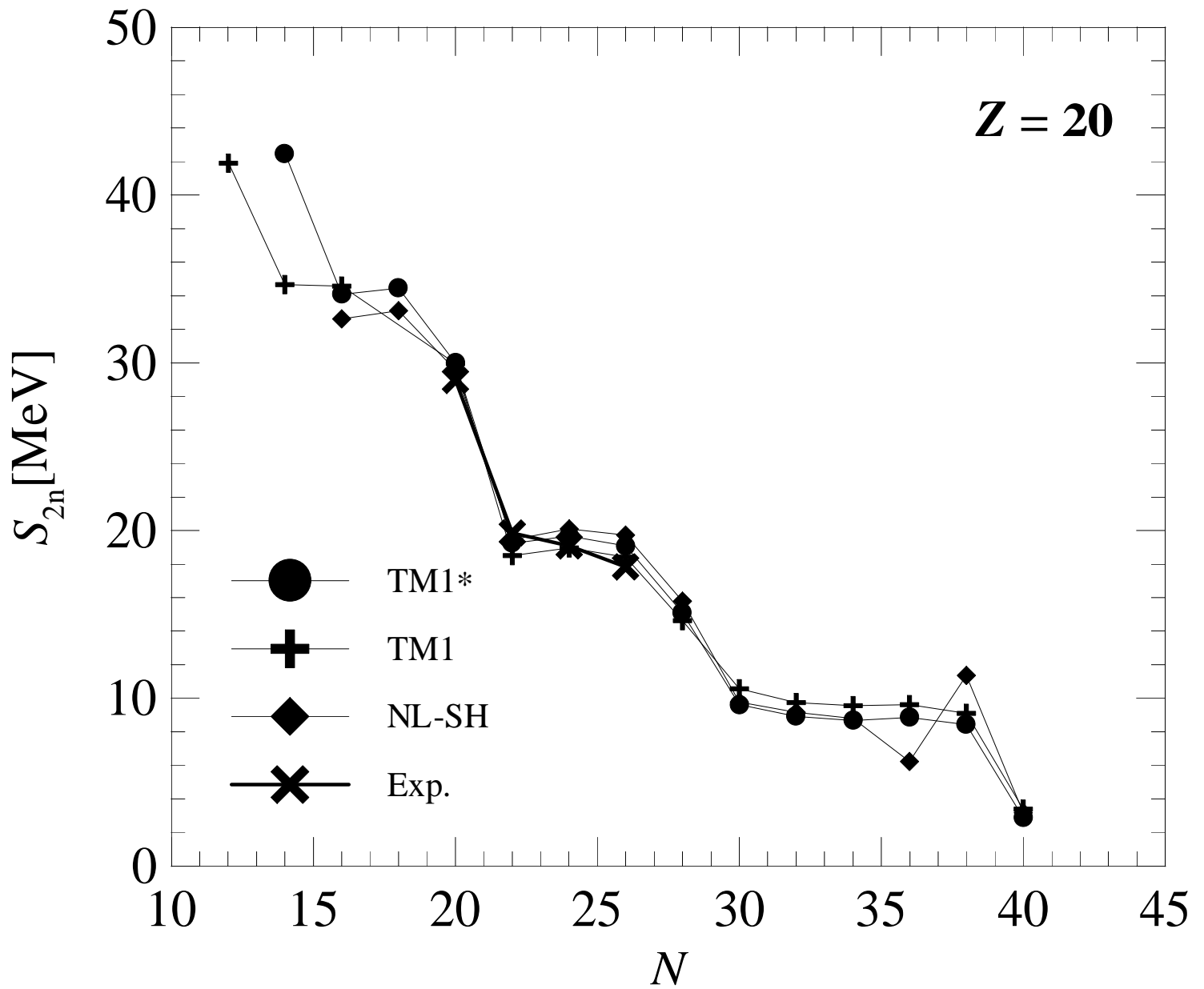


Figure 6b

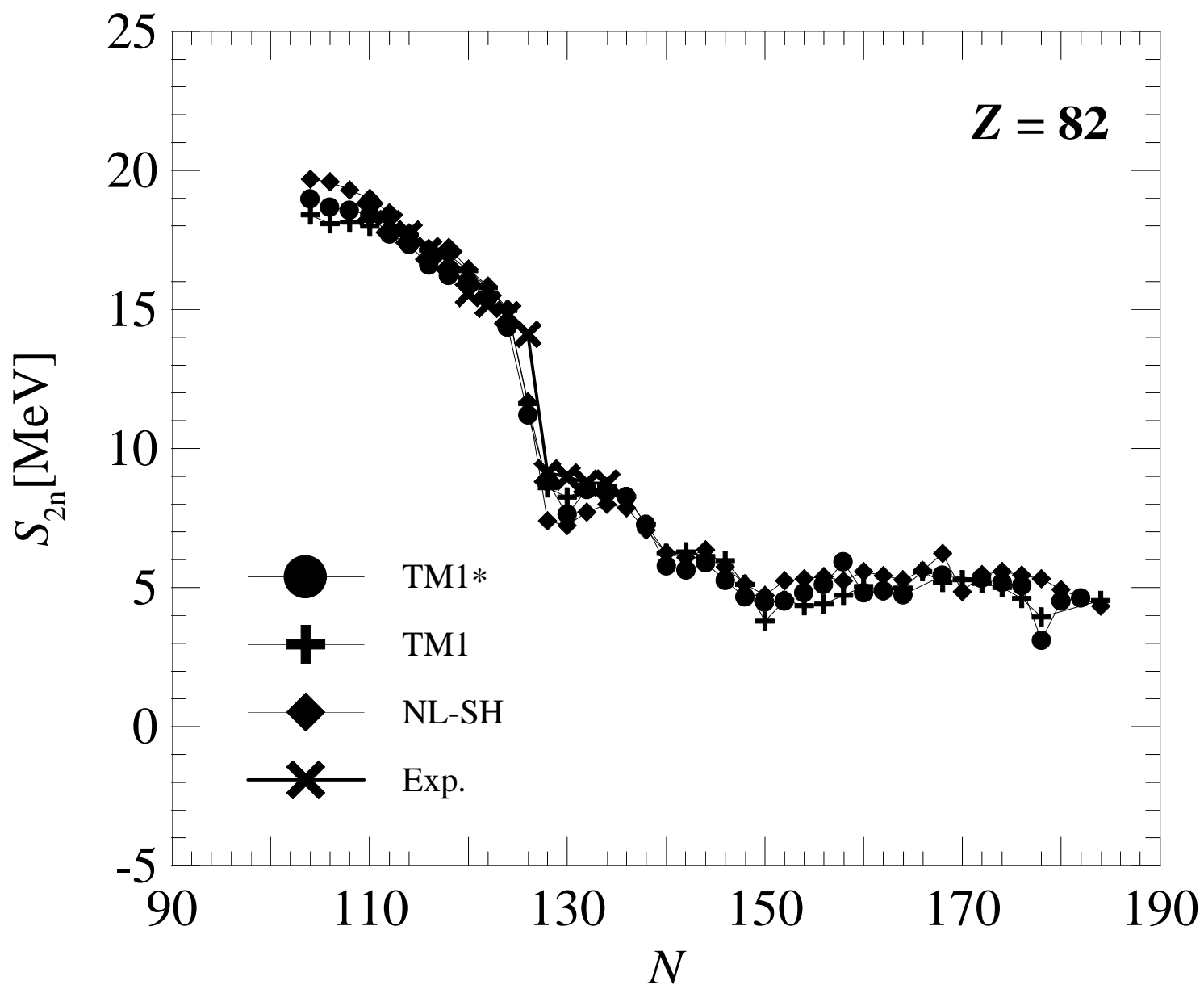


Figure 6c

